 SL, vol.6, no.2, pp.77-91, 2011

Discretisation of the velocity-pressure formulation with integrated radial-basis-function networks

N. Thai-Quang[1], K. Le-Cao[1], N. Mai-Duy[1] and T. Tran-Cong[1]

Abstract: This study is concerned with the use of integrated radial-basis-function networks (IRBFNs) for the discretisation of the velocity-pressure formulation in two dimensions on Cartesian grids. In the approximation of the field variables (i.e. velocity components and pressure), instead of using low-order polynomial interpolants, we employ global IRBFNs along grid lines (i.e. one-dimensional IRBFNs). In the imposition of boundary condition for the pressure, we propose two treatments, namely Treatment A and Treatment B. For both treatments, Neumann boundary conditions are transformed into Dirichlet ones. The former is based on values of the pressure at interior nodes along a grid line and first derivative values of the pressure at two extreme nodes of that grid line; while the latter relies on values of the pressure at interior nodes along a grid line together with both first and second derivative values of the pressure at two extreme nodes of that grid line. The proposed method is verified successfully through the simulation of a benchmark test, namely the isothermal lid-driven cavity flow problem.

Keywords: integrated radial basis function, pressure-velocity formulation, lid-driven cavity flow, Dirichlet boundary condition, Cartesian grid.

1 Introduction

It is known that the equations of motion of a Newtonian fluid can be written in several formulations including the velocity-pressure ($\widehat{u}-p$) formulation, the stream function-vorticity ($\psi-\omega$) formulation and the stream function (ψ) formulation. The last two involve less dependent variables than the first one. However, they require some special treatments for the handling of the vorticity boundary condition (the $\psi-\omega$ formulation) and the calculation of high-order derivatives including the cross-ones (the ψ formulation). Furthermore, the pressure field needs be resolved, which is generally recognised as a complicated process. For the $\widehat{u}-p$ formula-

[1] Computational Engineering and Science Research Centre, Faculty of Engineering and Surveying, The University of Southern Queensland, Toowoomba, Queensland 4350, Australia.

tion, the pressure and velocity fields are obtained directly from the discretisation equations and it is straightforward to extend the formulation to 3D problems.

It was reported in the literature (e.g. [Roache (1998); Cheng (1968);Cyrus and Fulton (1967)]) that the use of conservative form of the governing equation has the ability to give more accurate results than the use of non-conservative form, especially for problems where the conservative property is crucial. The reader is referred to [Cheng (1968)] for certain solutions of the Burgers equation, and [Cyrus and Fulton (1967)] for elliptic equations. In [Torrance, Davis, Eike, Gill, Gutman, Hsui, Lyons, and Zien (1972)], through the simulation of a flow in a cavity, it was shown that results by using the conservative equations and first-order accurate interpolants are better than those by using the non-conservative equations and second-order accurate interpolants.

To facilitate numerical calculation, the spatial domain needs be discretised. Generating a Cartesian grid, which is associated with finite-difference methods (FDMs), can be seen to be much more straightforward than generating a finite-element (FE) mesh, which is associated with FEMs and finite-volume (FV) methods.

Radial basis function networks (RBFNs) have been emerged as a powerful approximation tool. They have been applied for the solution of ordinary and differential partial equations. The RBF approximations representing the field variable can be constructed through differentiation (DRBFNs) [Kansa (1990), Kansa, Power, Fasshauer, and Ling (2004)] and integration (IRBFNs) [Mai-Duy and Tran-Cong (2001)]. The latter has extra power in the implementation of multiple boundary values.

Most numerical methods for solving viscous incompressible flow in the $\widehat{u} - p$ formulation utilize a fractional step approach, which is originally suggested by [Chorin (1968)]. The variations of this approach have been published in, for example, [Kim and Moin (1985), Van Kan (1986), Bell, Colella, and Glaz (1989), Perot (1993), Almgren (1996)]. In this study, we will propose a numerical projection method, based on Cartesian grids and 1D-IRBFNs, for the simulation of viscous incompressible flows in two dimensions. Boundary conditions for the pressure are taken in the form of Dirichlet type, and to do so, two treatments, i.e. Treatment A and Treatment B, are proposed. The main difference between these two lies in the number of derivative boundary values used. The performance of the proposed method is investigated numerically through the simulation of isothermal lid-driven cavity flow. Numerical results show that the proposed Dirichlet boundary form yields better accuracy than the usual Neumann boundary form, and Treatment B is more accurate than Treatment A.

The remainder of the paper is organised as follows. Section 2 and 3 briefly outline

the governing equations and the proposed method, respectively. In section 4, two boundary treatments for the pressure are described. Numerical results are reported in section 5, where comparisons with the benchmark solutions are made. Finally, concluding remarks are given in section 6.

2 Governing equations

The transient incompressible Navier-Stokes equations in non-dimensional conservative form can be expressed as follows.

Continuity equation:

$$\frac{\partial u}{\partial x}+\frac{\partial v}{\partial y}=0 \tag{1}$$

Momentum equations:

$$\frac{\partial u}{\partial t}+\frac{\partial (uu)}{\partial x}+\frac{\partial (vu)}{\partial y}=-\frac{\partial p}{\partial x}+\frac{1}{Re}\left(\frac{\partial^2 u}{\partial x^2}+\frac{\partial^2 u}{\partial y^2}\right) \tag{2}$$

$$\frac{\partial v}{\partial t}+\frac{\partial (uv)}{\partial x}+\frac{\partial (vv)}{\partial y}=-\frac{\partial p}{\partial y}+\frac{1}{Re}\left(\frac{\partial^2 v}{\partial x^2}+\frac{\partial^2 v}{\partial y^2}\right) \tag{3}$$

where u, v and p are the x and y velocity components and the static pressure, respectively; and $Re = UL/\nu$ the Reynolds number, in which ν is the kinematic viscosity, L a characteristic length and U a characteristic speed of the flow.

3 Reviews of 1D-IRBFNs and projection method

3.1 1D-IRBFNs

Consider an univariate function $f(x)$. The second-order derivative of f is decomposed into RBFs

$$\frac{\partial^2 f(x)}{\partial x^2}=\sum_{i=1}^{m} w_i G_i(x) \tag{4}$$

where m is the number of RBFs; $\{G_i(x)\}_{i=1}^{m}$ the set of RBFs; and $\{w_i\}_{i=1}^{m}$ the set of weights to be found. Approximations for the first-order derivative and the function itself are then obtained through integration

$$\frac{\partial f(x)}{\partial x}=\sum_{i=1}^{m} w_i H_i(x)+c_1 \tag{5}$$

$$f(x)=\sum_{i=1}^{m} w_i \overline{H}_i(x)+c_1 x+c_2 \tag{6}$$

where $H_i(x) = \int G_i(x)dx$; $\overline{H}_i(x) = \int H_i(x)dx$; and c_1 and c_2 are the constants of integration with respect to x.

Let $\{x_i\}_{i=1}^{q}$ and $\{x_{b1}, x_{b2}\}$ be a set of interior points and a set of boundary points, respectively. We choose the set of centres as the set of nodal points. Evaluation of (6) at interior and boundary points results in

$$\begin{pmatrix} \widehat{f} \\ \widehat{f}_b \end{pmatrix} = \overline{\mathscr{H}} \begin{pmatrix} \widehat{w} \\ c_1 \\ c_2 \end{pmatrix} \tag{7}$$

where $m = q+2$

$$\begin{aligned} \widehat{f} &= (f_1, f_2, \cdots, f_q)^T \\ \widehat{f}_b &= (f_{b1}, f_{b2})^T \\ \widehat{w} &= (w_1, w_2, \cdots, w_m)^T \\ \overline{\mathscr{H}} &= \begin{bmatrix} \overline{H}_1(x_1) & \cdots & \overline{H}_m(x_1) & x_1 & 1 \\ \overline{H}_1(x_2) & \cdots & \overline{H}_m(x_2) & x_2 & 1 \\ \vdots & \ddots & \vdots & \vdots & \vdots \\ \overline{H}_1(x_q) & \cdots & \overline{H}_m(x_q) & x_q & 1 \\ \overline{H}_1(x_{b1}) & \cdots & \overline{H}_m(x_{b1}) & x_{b1} & 1 \\ \overline{H}_1(x_{b2}) & \cdots & \overline{H}_m(x_{b2}) & x_{b2} & 1 \end{bmatrix} \end{aligned} \tag{8}$$

The obtained system (7) for the unknown vector of network weights $(\widehat{w}, c_1, c_2)$ can be solved using the singular value decomposition (SVD) technique

$$\begin{pmatrix} \widehat{w} \\ c_1 \\ c_2 \end{pmatrix} = \overline{\mathscr{H}}^{-1} \begin{pmatrix} \widehat{f} \\ \widehat{f}_b \end{pmatrix} \tag{9}$$

where $\overline{\mathscr{H}}^{-1}$ is the pseudo-inverse of $\overline{\mathscr{H}}$.

Making use of (9), (5) and (4), the values of the first and second derivatives of f at the interior and boundary points are respectively computed as

$$\begin{pmatrix} \frac{\partial f_1}{\partial x} \\ \frac{\partial f_2}{\partial x} \\ \vdots \\ \frac{\partial f_q}{\partial x} \\ \frac{\partial f_{b1}}{\partial x} \\ \frac{\partial f_{b2}}{\partial x} \end{pmatrix} = \begin{bmatrix} H_1(x_1) & \cdots & H_m(x_1) & 1 & 0 \\ H_1(x_2) & \cdots & H_m(x_2) & 1 & 0 \\ \vdots & \ddots & \vdots & \vdots & \vdots \\ H_1(x_q) & \cdots & H_m(x_q) & 1 & 0 \\ H_1(x_{b1}) & \cdots & H_m(x_{b1}) & 1 & 0 \\ H_1(x_{b2}) & \cdots & H_m(x_{b2}) & 1 & 0 \end{bmatrix} \overline{\mathscr{H}}^{-1} \begin{pmatrix} \widehat{f} \\ \widehat{f}_b \end{pmatrix} \tag{10}$$

$$\begin{pmatrix} \frac{\partial^2 f_1}{\partial x^2} \\ \frac{\partial^2 f_2}{\partial x^2} \\ \vdots \\ \frac{\partial^2 f_q}{\partial x^2} \\ \frac{\partial^2 f_{b1}}{\partial x^2} \\ \frac{\partial^2 f_{b2}}{\partial x^2} \end{pmatrix} = \begin{bmatrix} G_1(x_1) & \cdots & G_m(x_1) & 0 & 0 \\ G_1(x_2) & \cdots & G_m(x_2) & 0 & 0 \\ \vdots & \ddots & \vdots & \vdots & \vdots \\ G_1(x_q) & \cdots & G_m(x_q) & 0 & 0 \\ G_1(x_{b1}) & \cdots & G_m(x_{b1}) & 0 & 0 \\ G_1(x_{b2}) & \cdots & G_m(x_{b2}) & 0 & 0 \end{bmatrix} \overline{\mathscr{H}}^{-1} \begin{pmatrix} \widehat{f} \\ \widehat{f}_b \end{pmatrix} \tag{11}$$

or in compact form

$$\widehat{\frac{\partial f}{\partial x}} = \widehat{\mathscr{D}}_{1x}\widehat{f} + \widehat{k}_{1x}, \tag{12}$$

and

$$\widehat{\frac{\partial^2 f}{\partial x^2}} = \widehat{\mathscr{D}}_{2x}\widehat{f} + \widehat{k}_{2x}, \tag{13}$$

where the matrices $\widehat{\mathscr{D}}_{1x}$ and $\widehat{\mathscr{D}}_{2x}$ consist of all but the last two columns of the product of two matrices on the right-hand side of (10) and (11); and $\widehat{k}_{1x}$ and $\widehat{k}_{2x}$ are obtained by multiplying the vector $\widehat{f}_b$ with the last two columns. It is noted that $\widehat{k}_{1x}$ and $\widehat{k}_{2x}$ are vectors of known quantities related to boundary conditions.

The above 1D-IRBFNs expressions for the function derivatives are now written in terms of nodal values of f.

3.2 Projection method

Equations (1)-(3) can be rewritten in vector form as

$$\nabla.\widehat{u} = 0 \tag{14}$$

$$\frac{\partial \widehat{u}}{\partial t} + \nabla.(\widehat{u}\,\widehat{u}) = -\nabla p + \frac{1}{Re}\nabla^2\widehat{u} \tag{15}$$

In the projection method, the velocity and pressure equations are solved separately in each iteration. Discretisation of (15) with an explicit Euler scheme gives

$$\frac{\widehat{u}^{n+1} - \widehat{u}^n}{\Delta t} = -\nabla p^{n+1} + \frac{1}{Re}\nabla^2\widehat{u}^n - \nabla.(\widehat{u}^n\widehat{u}^n) \tag{16}$$

An intermediate velocity vector, denoted by $\widehat{u}^*$, is computed by neglecting the pressure gradient term on the RHS of (16).

$$\frac{\widehat{u}^* - \widehat{u}^n}{\Delta t} = \frac{1}{Re}\nabla^2\widehat{u}^n - \nabla.(\widehat{u}^n\widehat{u}^n) \tag{17}$$

or

$$\widehat{u}^* = \widehat{u}^n + \Delta t(\frac{1}{Re}\nabla^2\widehat{u}^n - \nabla.(\widehat{u}^n\widehat{u}^n) \tag{18}$$

It is seen that $\widehat{u}^*$ does not satisfy the continuity equation.

From (16) and (17), one can derive the following equation

$$\frac{\widehat{u}^{n+1} - \widehat{u}^*}{\Delta t} = -\nabla p^{n+1} \tag{19}$$

The pressure Poisson equation is obtained by applying the gradient operator to both sides of (19) and forcing $\widehat{u}^{n+1}$ to satisfy the continuity equation

$$\nabla^2 p^{n+1} = \frac{1}{\Delta t}\nabla \cdot \widehat{u}^* \tag{20}$$

After solving (20), the velocity field at the next time level is calculated through (19) as

$$\widehat{u}^{n+1} = \widehat{u}^* - \Delta t \nabla p^{n+1} \tag{21}$$

4 Proposed method

It has generally been accepted that, among RBFs, the multiquadric (MQ) scheme tends to result in the most accurate approximation [Franke (1982)]. We choose MQ as the basis function in the present calculation.

The problem domain is discretised using a Cartesian grid. On each grid line,

- 1D-IRBFNs are employed to represent the variations of the velocity components, the intermediate velocity components and the pressure
- values of the pressure at the two extreme are estimated and they are used as Dirichlet boundary conditions for the pressure Poisson equation (20)

In the following, the solution procedure is first outlined and the two boundary treatments for the pressure are then presented.

4.1 Solution procedure

At each time step, the following calculations are required

- Compute the diffusion term $\nabla^2\widehat{u}^n$ and the convection term $\nabla.(\widehat{u}^n\widehat{u}^n)$ using 1D-IRBFNs

- Compute the intermediate velocity field $\widehat{u}^*$

$$\widehat{u}^* = \widehat{u}^n + \Delta t(\frac{1}{Re}\nabla^2\widehat{u}^n - \nabla.(\widehat{u}^n\widehat{u}^n) \tag{22}$$

- Compute boundary derivative values of the pressure from the momentum equations

$$\frac{\partial p^{n+1}}{\partial \widehat{n}} = \frac{1}{\Delta t}(\widehat{u}^* - \widehat{u}^n) \tag{23}$$

- Derive a Dirichlet boundary condition for the pressure using Treatment A and Treatment B
- Compute $\nabla.\widehat{u}^*$ using 1D-IRBFNs
- Solve the pressure Poisson equation

$$\nabla^2 p^{n+1} = \frac{1}{\Delta t}\nabla.\widehat{u}^* \tag{24}$$

  subject to Dirichlet boundary conditions

- Compute ∇p^n using 1D-IRBFNs
- Estimate the velocity field at the next time level

$$\widehat{u}^{n+1} = \widehat{u}^* - \Delta t(\nabla p^n) \tag{25}$$

4.2 Pressure boundary treatments

As mentioned earlier, for both Treatment A and Treatment B, Neumann boundary conditions are transformed into Dirichlet ones. The former is based on values of the pressure at interior nodes along a grid line and first derivative values of the pressure at two extreme nodes of that grid line; while the latter relies on values of the pressure at interior nodes along a grid line together with both first and second derivative values of the pressure at two extreme nodes of that grid line.

4.2.1 Treatment A

On a x-grid line, the system that represents the relationship between the RBF space and the physical space (i.e. the conversion system) can be established as

$$\begin{pmatrix} \widehat{p} \\ \frac{\partial p_{b1}}{\partial x} \\ \frac{\partial p_{b2}}{\partial x} \end{pmatrix} = \begin{pmatrix} \overline{\mathscr{H}} \\ \mathscr{H} \end{pmatrix} \begin{pmatrix} \widehat{w} \\ c_1 \\ c_2 \end{pmatrix} \tag{26}$$

or

$$\begin{pmatrix} \widehat{w} \\ c_1 \\ c_2 \end{pmatrix} = \begin{pmatrix} \overline{\mathscr{H}} \\ \mathscr{H} \end{pmatrix}^{-1} \begin{pmatrix} \widehat{p} \\ \frac{\partial p_{b1}}{\partial x} \\ \frac{\partial p_{b2}}{\partial x} \end{pmatrix} \tag{27}$$

where

$$\widehat{p} = (p_1, p_2, \cdots, p_q)^T$$
$$\widehat{w} = (w_1, w_2, \cdots, w_m)^T$$

$$\overline{\mathscr{H}} = \begin{bmatrix} \overline{H}_1(x_1) & \cdots & \overline{H}_m(x_1) & x_1 & 1 \\ \overline{H}_1(x_2) & \cdots & \overline{H}_m(x_2) & x_2 & 1 \\ \vdots & \ddots & \vdots & \vdots & \\ \overline{H}_1(x_q) & \cdots & \overline{H}_m(x_q) & x_q & 1 \end{bmatrix} \tag{28}$$

$$\mathscr{H} = \begin{bmatrix} H_1(x_{b1}) & \cdots & H_m(x_{b1}) & 1 & 0 \\ H_1(x_{b2}) & \cdots & H_m(x_{b2}) & 1 & 0 \end{bmatrix} \tag{29}$$

The nodal values of p at the two boundary nodes are then obtained by collocating (6) at x_{b1} and x_{b2} and making use of (27)

$$\begin{pmatrix} p_{b1} \\ p_{b2} \end{pmatrix} = \begin{bmatrix} \overline{H}_1(x_{b1}) & \cdots & \overline{H}_{nx}(x_{b1}) & x_{b1} & 1 \\ \overline{H}_1(x_{b2}) & \cdots & \overline{H}_{nx}(x_{b2}) & x_{b2} & 1 \end{bmatrix} \begin{pmatrix} \overline{\mathscr{H}} \\ \mathscr{H} \end{pmatrix}^{-1} \begin{pmatrix} \widehat{p} \\ \frac{\partial p_{b1}}{\partial x} \\ \frac{\partial p_{b2}}{\partial x} \end{pmatrix} \tag{30}$$

For a y-grid line, in the same way, one obtains nodal values of p at the two boundary nodes y_{b1} and y_{b2}.

4.2.2 Treatment B

On a x-grid line, the conversion matrix is established as

$$\begin{pmatrix} \widehat{p} \\ \frac{\partial p_{b1}}{\partial x} \\ \frac{\partial p_{b2}}{\partial x} \\ \frac{\partial^2 p_{b1}}{\partial x^2} \\ \frac{\partial^2 p_{b2}}{\partial x^2} \end{pmatrix} = \begin{pmatrix} \overline{\mathscr{H}} \\ \mathscr{H} \\ \mathscr{G} \end{pmatrix} \begin{pmatrix} \widehat{w} \\ c_1 \\ c_2 \end{pmatrix} \tag{31}$$

or

$$\begin{pmatrix} \widehat{w} \\ c_1 \\ c_2 \end{pmatrix} = \begin{pmatrix} \overline{\mathscr{H}} \\ \mathscr{H} \\ \mathscr{G} \end{pmatrix}^{-1} \begin{pmatrix} \widehat{p} \\ \frac{\partial p_{b1}}{\partial x} \\ \frac{\partial p_{b2}}{\partial x} \\ \frac{\partial^2 p_{b1}}{\partial x^2} \\ \frac{\partial^2 p_{b2}}{\partial x^2} \end{pmatrix} \tag{32}$$

where

$$\widehat{p} = (p_1, p_2, \cdots, p_q)^T$$
$$\widehat{w} = (w_1, w_2, \cdots, w_m)^T$$

$$\overline{\mathscr{H}} = \begin{bmatrix} \overline{H}_1(x_1) & \cdots & \overline{H}_m(x_1) & x_1 & 1 \\ \overline{H}_1(x_2) & \cdots & \overline{H}_m(x_2) & x_2 & 1 \\ \vdots & \ddots & \vdots & \vdots & \\ \overline{H}_1(x_q) & \cdots & \overline{H}_m(x_q) & x_q & 1 \end{bmatrix} \tag{33}$$

$$\mathscr{H} = \begin{bmatrix} H_1(x_{b1}) & \cdots & H_m(x_{b1}) & 1 & 0 \\ H_1(x_{b2}) & \cdots & H_m(x_{b2}) & 1 & 0 \end{bmatrix} \tag{34}$$

$$\mathscr{G} = \begin{bmatrix} G_1(x_{b1}) & \cdots & G_m(x_{b1}) & 0 & 0 \\ G_1(x_{b2}) & \cdots & G_m(x_{b2}) & 0 & 0 \end{bmatrix} \tag{35}$$

It leads to

$$\begin{pmatrix} p_{b1} \\ p_{b2} \end{pmatrix} = \begin{bmatrix} \overline{H}_1(x_{b1}) & \cdots & \overline{H}_m(x_{b1}) & x_{b1} & 1 \\ \overline{H}_1(x_{b2}) & \cdots & \overline{H}_m(x_{b2}) & x_{b2} & 1 \end{bmatrix} \begin{pmatrix} \overline{\mathscr{H}} \\ \mathscr{H} \\ \mathscr{G} \end{pmatrix}^{-1} \begin{pmatrix} \widehat{p} \\ \frac{\partial p_{b1}}{\partial x} \\ \frac{\partial p_{b2}}{\partial x} \\ \frac{\partial^2 p_{b1}}{\partial x^2} \\ \frac{\partial^2 p_{b2}}{\partial x^2} \end{pmatrix} \tag{36}$$

For a y-grid line, nodal values of p at the two boundary nodes can be obtained in a similar manner.

It is noted that when the convection term vanishes on the boundary, e.g. walls in a lid-driven cavity flow problem, boundary derivative values for the pressure can be

calculated as

$$\frac{\partial p_b}{\partial x} = \frac{1}{Re}\left(\frac{\partial^2 u_b}{\partial x^2} + \frac{\partial^2 u_b}{\partial y^2}\right) \tag{37}$$

$$\frac{\partial p_b}{\partial y} = \frac{1}{Re}\left(\frac{\partial^2 v_b}{\partial x^2} + \frac{\partial^2 v_b}{\partial y^2}\right) \tag{38}$$

5 Numerical results

The isothermal lid-driven cavity flow has been widely used as a test problem for the assessment of accuracy of numerical solvers in CFD. From the literature, FD results using very dense grids by Ghia, Ghia, and Shin (1982) and pseudo-spectral results by Botella and Peyret (1998) have been often cited for comparison purposes. It is noted that for the latter, the field variable was decomposed into the regular part that is approximated with Chebyshev polynomials and the singular part that is treated analytically; and a benchmark spectral solution for $R_e = 100$ and $R_e = 1000$ were provided.

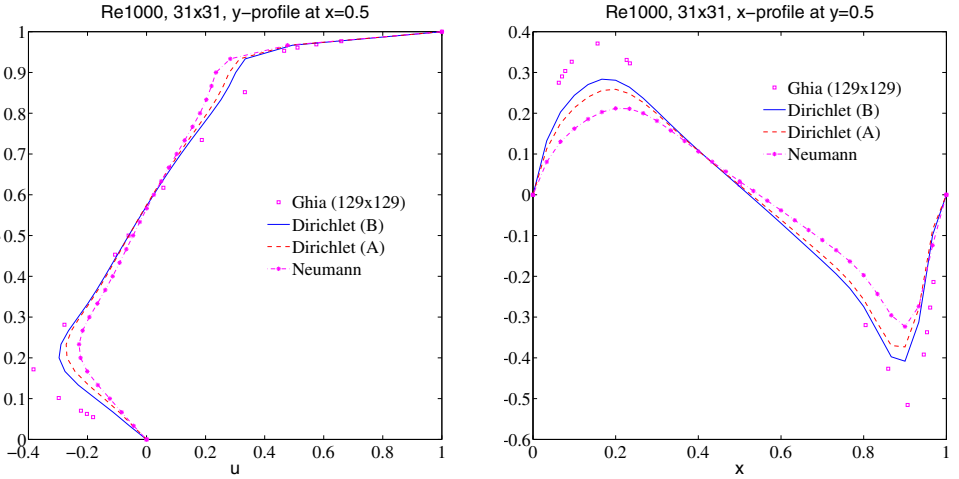

Figure 1: Comparison of the velocity profiles of the flow at $R_e = 1000$ by the IRBFN method between the two proposed treatments (Treatment A and Treatment B) and the usual treatment (i.e. Neumann boundary condition). Results obtained by the FDM [Ghia, Ghia, and Shin (1982)] are also included.

Figure 1 shows a comparison of the velocity profiles of the flow at $R_e = 1000$ by the IRBFN method between the two proposed treatments (Treatment A and Treatment B) and the usual treatment (i.e. Neumann boundary condition). Note that a coarse grid is used to accentuate the difference between results. It can be seen that the former is in closer agreement with the FD results than the latter. Moreover, Treatment B performs better than Treatment A.

The IRBFNs results of velocity are compared with the benchmark finite-difference and spectral solutions and some other published solutions in Tables 1 and 2. It can be seen that the present results are in good agreement with the spectral solutions, even at relative coarse grids. Some plots of velocity profiles for $R_e = 100$, $R_e = 400$, $R_e = 1000$ are shown in Figures 2, 3 and 4.

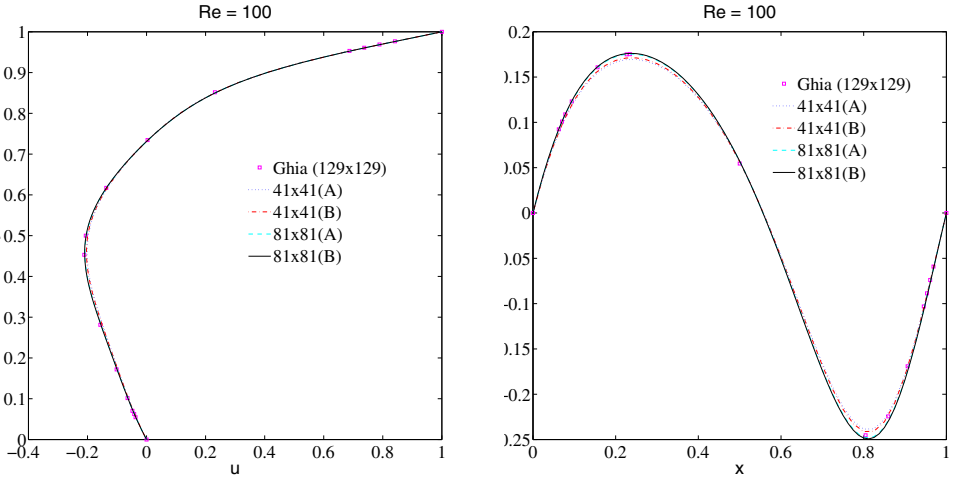

Figure 2: Comparison of the velocity profiles of the flow at $R_e = 100$ between the present method (Treatment A and Treatment B with two grids) and the FDM.

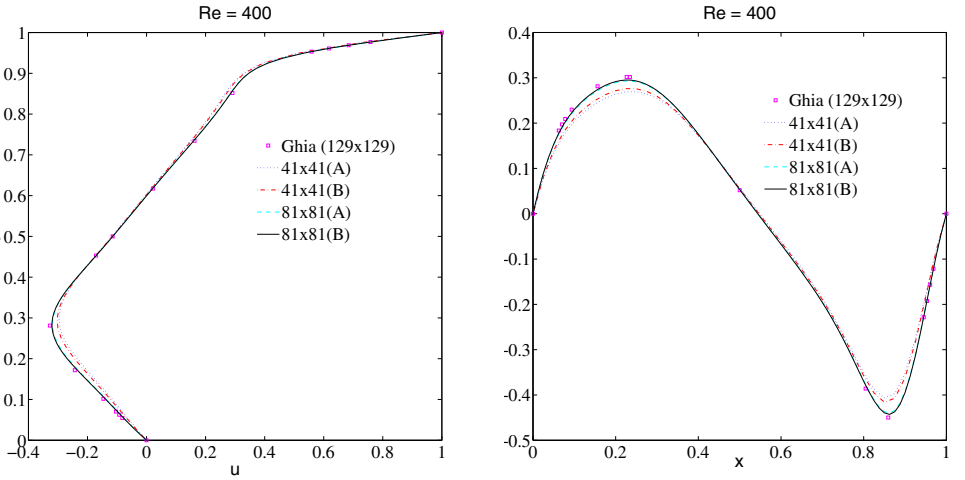

Figure 3: Comparison of the velocity profiles of the flow at $R_e = 400$ between the present method (Treatment A and Treatment B with two grids) and the FDM.

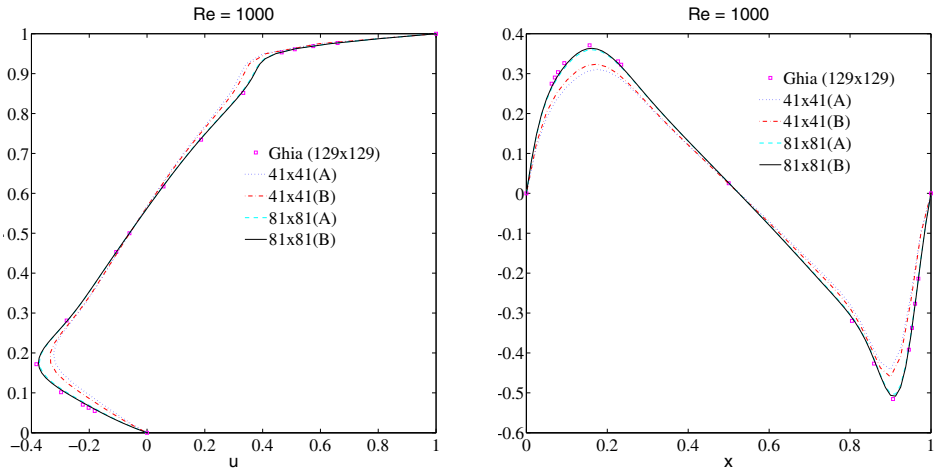

Figure 4: Comparison of the velocity profiles of the flow at $R_e = 1000$ between the present method (Treatment A and Treatment B with two grids) and the FDM.

Figure 5 displays the static pressure field for $R_e = 100$ and $R_e = 400$, which look feasible when compared with those reported in Abdallah (1987). It is noted that the static pressure coefficient $C_{p,s}$ is defined as $C_{p,s} = 2(P_s - P_c)/U^2$, where P_c is the static pressure at the center of the cavity lower wall and U is the reference velocity. When compared with pseudo-spectral techniques, attractive features of the present 1D-IRBFNs technique are that it does not require any special treatments for the corner singularity and it can work with uniform grids.

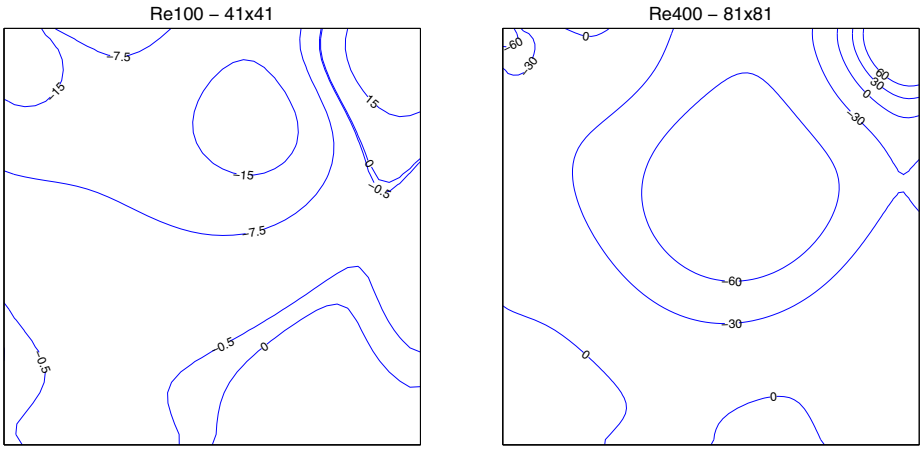

Figure 5: Contour plots of the static pressure $ReC_{p,s}$ for $R_e = 100$ (left) and $R_e = 400$ (right).

Table 1: Lid-driven cavity flow, $R_e = 100$: extrema of the vertical and horizontal velocity profiles through the centre of the cavity

Method	Grid	u_{min}	Error (%)	y_{min}	v_{max}	error (%)	x_{max}	v_{min}	error (%)	x_{min}
Present (Treatment A)	41x41	-0.2014888	5.865	0.4596	0.1696241	5.540	0.2396	-0.239526	5.625	0.8118
Present (Treatment B)	41x41	-0.2038341	4.769	0.4593	0.1714081	4.547	0.2391	-0.242257	4.549	0.8114
Present (Treatment A)	81x81	-0.2086177	2.534	0.4581	0.1753851	2.332	0.2381	-0.248226	2.197	0.8112
Present (Treatment B)	81x81	-0.2096592	2.048	0.4581	0.1761823	1.888	0.2379	-0.249317	1.767	0.8110
FDM($\psi - \omega$) [Ghia]	129x129	-0.2109	1.468	0.4531	0.17527	2.396	0.2344	-0.24533	3.338	0.8047
FDM($\widehat{u} - p$) [Bruneau]	129x129	-0.2106	1.608	0.4531	0.1786	0.542	0.2344	-0.2521	0.671	0.8125
FVM($\widehat{u} - p$) [Sahin]	257x257	-0.213924	0.055	0.4598	0.180888	0.732	0.2354	-0.256603	1.103	0.8127
FVM($\widehat{u} - p$) [Deng]	64x64	-0.21315	0.417	—	0.17896	0.341	—	-0.25339	0.163	—
Benchmark [Botella]		-0.2140424		0.4581	0.1795728		0.2370	-0.253803		0.8104

Table 2: Lid-driven cavity flow, $R_e = 1000$: extrema of the vertical and horizontal velocity profiles through the centre of the cavity

Method	Grid	u_{min}	Error (%)	y_{min}	v_{max}	error (%)	x_{max}	v_{min}	error (%)	x_{min}
Present (Treatment A)	41x41	-0.3238302	16.661	0.1955	0.3106138	17.597	0.1756	-0.4425082	16.045	0.8959
Present (Treatment B)	41x41	-0.3362997	13.452	0.1890	0.3239604	14.056	0.1700	-0.4606564	12.602	0.8973
Present (Treatment A)	81x81	-0.3722885	4.190	0.1769	0.3598330	4.540	0.1624	-0.5052874	4.134	0.9072
Present (Treatment B)	81x81	-0.3756913	3.314	0.1754	0.3633996	3.593	0.1612	-0.5099789	3.244	0.9077
FDM ($\psi - \omega$) [Ghia]	129x129	-0.38289	1.462	0.1719	0.37095	1.590	0.8437	-0.5155	2.196	0.9063
FDM ($\widehat{u} - p$) [Bruneau]	256x256	-0.3764	3.132	0.1602	0.3665	2.771	0.8477	-0.5208	1.191	0.9102
FVM($\widehat{u} - p$),stagg. [Deng]	128x128	-0.3805	2.077	—	0.36884	2.150	—	-0.51727	1.861	—
FVM($\widehat{u} - p$)cpi [Deng]	128x128	-0.38511	0.890	—	0.37369	0.863	—	-0.5228	0.811	—
Benchmark [Botella]		-0.3885698		0.1717	0.3769447		0.1578	-0.5270771		0.0908

6 Concluding remarks

This paper reports a projection technique, based on point collocation, 1D-IRBFNs and Cartesian grids, for the discretisation of the velocity-pressure formulation in conservative form. Two effective treatments are proposed to transform a Neumann boundary condition of the pressure into a Dirichlet one. Numerical results of the lid-driven cavity flow problem indicate that (i) the IRBFN solutions agree well with those published in the literature, (ii) the use of a Dirichlet boundary form outperforms the use of a Neumann boundary form, and (iii) Treatment B is more accurate than Treatment A.

Acknowledgement: The first author would like to thank USQ, FoES and CESRC for a postgraduate research scholarship. This work was supported by the Australian Research Council.

References

Abdallah, S. (1987): Numerical solutions for the incompressible navier-stokes equations in primitive variables using a non-staggered grid, II. *Journal of Computational Physics*, vol. 70, no. 1, pp. 193–202.

Almgren, A. S. (1996): A numerical method for the incompressible navier-stokes equations based on an approximate projection. *SIAM J. Sci. Compt.*, vol. 17.

Bell, J.; Colella, P.; Glaz, H. (1989): A second-order projection method for the incompressible navier-stokes equations. *Journal of Computational Physics*, vol. 85, no. 2, pp. 257–283.

Botella, O.; Peyret, R. (1998): Benchmark spectral results on the lid-driven cavity flow. *Computers & Fluids*, vol. 27, no. 4, pp. 421–433.

Cheng, S. I. (1968): *Accuracy of difference formulation of Navier-Stokes equations*. A. M. S. Department, Princeton University, Princeton, New Jersey.

Chorin, A. (1968): Numerical solution of the navier-stokes equations. *Mathematics of Computation*, vol. 22, no. 104, pp. 745–762.

Cyrus, N. J.; Fulton, R. E. (1967): *Accuracy study of finite difference methods*. NASA TN D-4372, National Aeronautics and Space Administration, Langley Research Centre, Langley Station, Hampton, Virginia.

Franke, R. (1982): Scattered data interpolation: Tests of some method. *Mathematics of Computation*, vol. 38, pp. 181–200.

Ghia, U.; Ghia, K. N.; Shin, C. (1982): High-re solutions for incompressible flow using the navier-stokes equations and a multigrid method. *Journal of Computational Physics*, vol. 48, no. 3, pp. 387–411.

Kansa, E. J. (1990): Multiquadrics- A scattered data approximation scheme with applications to computational fluid-dynamics-I. surface approximations and partial derivative estimates. *Computers and Mathematics with Applications*, vol. 19, no. 8/9, pp. 127–145.

Kansa, E. J.; Power, H.; Fasshauer, G. E.; Ling, L. (2004): A volumetric integral radial basis function method for time-dependent partial differential equations: I formulation. *Engineering Analysis with Boundary Elements*, vol. 28, pp. 1191–1206.

Kim, J.; Moin, P. (1985): Application of a fractional-step method to incompressible navier-stokes equations. *Journal of Computational Physics*, vol. 59, no. 2, pp. 308–323.

Mai-Duy, N.; Tran-Cong, T. (2001): Numerical solution of differential equations using multiquadric radial basic function networks. *Neural Networks*, vol. 14, pp. 185–199.

Perot, J. (1993): An analysis of the fractional step method. *Journal of Computational Physics*, vol. 108, no. 1, pp. 51–58.

Roache, P. J. (1998): *Fundamentals of Computational Fluid Dynamics*. Hermosa Publishers.

Torrance, K.; Davis, R.; Eike, K.; Gill, P.; Gutman, D.; Hsui, A.; Lyons, S.; Zien, H. (1972): Cavity flows driven by bouyancy and shear. *Journal of Fluid Mechanics*, vol. 51, no. part2, pp. 221–231.

Van Kan, J. (1986): A second-order accurate pressure-correction scheme for viscous incompressible flow. *SIAM Journal on Scientific and Statistical Computing*, vol. 7, pp. 870.